

Microscopic optical potentials for nucleon-nucleus scattering

S. Karataglidis and M. B. Chadwick

Theoretical Division, Los Alamos National Laboratory, Los Alamos, NM, 87545

(October 29, 2018)

Abstract

Microscopic optical potentials for nucleon-nucleus (NA) scattering obtained from the folding of the effective g matrices, solutions of the Bruckner-Bethe-Goldstone equation, with the densities of the target, are applied to the case of neutron-nucleus scattering. Given that the optical potentials are specified in all two-body angular momentum, spin and isospin channels available to the NA scattering, the only difference in this model description of proton and neutron scattering observables for a given nucleus is in the inclusion of the Coulomb interaction. *A priori* microscopic optical model predictions for neutron and proton elastic scattering are compared with results from a phenomenological optical model and with data. New measurements are recommended to reduce discrepancies in the existing database, and to differentiate between different theoretical predictions.

arXiv:nucl-th/0104049v2 23 Aug 2001

I. INTRODUCTION

All of the development of the folding models of the microscopic nucleon-nucleus (NA) optical potentials for medium energy scattering to date have concentrated on the description of proton-nucleus (pA) scattering observables, with particular emphasis on studying the effective interaction and its components (see Ref. [1] and references cited therein). Much success in the description of differential cross sections and spin observables has been achieved by using a folding model in the coordinate space representation when coupled with reasonable models of nuclear structure [2]. More recently, this model has also been applied to the predictions of integral observables, with success in describing data from both proton and neutron scattering [3].

A natural extension of the application of this formalism would be to describe the observables for neutron-nucleus (nA) scattering. Comparison of nA and pA data for a given target and at a given energy would elicit details specifically of the nuclear part of the microscopic optical potential. Such a comparison would also highlight the role of the Coulomb interaction in NA scattering. It is only the inclusion (or exclusion) of the Coulomb interaction being the only difference in proton and neutron scattering that results in the prediction that the analyzing powers for neutron and proton elastic scattering from ^{208}Pb at 100 MeV would be completely out of phase [4]. This phenomenological result has yet to be experimentally verified so it would be instructive to note if a completely microscopic model for the scattering would lead to the same conclusion. Such was done for 100 MeV scattering by Karataglidis and Madland [5], whose results supported the phenomenological result.

Reaction and scattering information can be obtained directly from the optical model. However, while numerous measurements have been made for proton reaction cross sections and elastic scattering distributions, very few measurements have been made for neutrons above 20 MeV, owing to experimental difficulties in producing suitable monoenergetic neutron beams. Thus, phenomenological proton optical potentials can be obtained from fitting the available proton scattering data, but this approach cannot be directly used to obtain phenomenological neutron potentials, though procedures exist by which the neutron potential may be obtained from that of the proton using a Lane model. Therefore, we look to the applicability of the microscopic NA optical potentials to nA scattering.

A microscopic theory of NA scattering must necessarily start with an appropriate form of the underlying nucleon-nucleon (NN) interaction from which the g matrices for nucleons scattering from infinite nuclear matter are obtained as solutions of the Bruckner-Bethe-Goldstone (BBG) equation. A local density approximation then maps the g matrix onto an effective NN interaction in medium for the target in question. That effective interaction is folded with density of the target to obtain the microscopic, nonlocal, optical potential, cast in terms of central, tensor and spin-orbit terms. For the calculations presented herein, we use the Bonn B [6] NN interaction as the starting interaction, with densities obtained primarily from the shell model, specifying both the density dependence of the effective NA interaction and the density of the target.

The examples considered herein are 65 MeV proton and neutron scattering from ^{12}C , ^{28}Si , ^{40}Ca , ^{56}Fe , ^{90}Zr , and ^{208}Pb . These choices are predicated on the availability of both proton and neutron scattering data. Comparisons of the results of the microscopic calculations are also made with results obtained using a global phenomenological optical potential applicable

for the mass range encompassed in our investigation.

II. OPTICAL POTENTIALS

The complete details of the calculation of the microscopic optical potential can be found in a recent review article [1], including details of the program DWBA98 [7], with which we calculate the optical potential and all observables. Herein, we present a summary showing the relevant details to allow for a comparison of pA and nA scattering.

With \vec{r} and \vec{r}' denoting the relative coordinates between a colliding pair of particles, the Schrödinger equation describing their scattering by a local Coulomb, $V_C(r)$, and a nonlocal hadronic (optical) potential is of the form

$$\left[\frac{\hbar^2}{2\mu} \nabla^2 - V_C(r) + E \right] \Psi(\vec{r}) = \int U(\vec{r}, \vec{r}') \Psi(\vec{r}') d\vec{r}' , \quad (1)$$

where $\Psi(\vec{r})$ is the scattering solution and $U(\vec{r}, \vec{r}')$ is the optical potential. The optical potential is obtained by the folding of the relevant nuclear structure information with the effective g matrices, as specified in ST -channel form and in coordinate space. They are obtained from the set of infinite matter nuclear g matrices [8,9] obtained by solution of the BBG equation,

$$g_{LL'}^{(JST)}(p', p; k, K, k_F) = V_{LL'}^{(JST)}(p, p') + \frac{2}{\pi} \sum_l \int_0^\infty V_{Ll}^{(JST)}(p', q) [\mathcal{H}] g_{lL'}^{(JST)}(q, p; k, K, k_F) q^2 dq , \quad (2)$$

where

$$\mathcal{H}(q, k, K, k_F) = \frac{\bar{Q}(q, K, k_F)}{\bar{E}(k, K, k_F) - \bar{E}(q, K, k_F) + i\varepsilon} \quad (3)$$

in which $\bar{Q}(q, K, k_F)$ is an angle-averaged Pauli operator with an average center-of-mass momentum K [8,9]. The energies in the propagator of the BBG equation include auxiliary potentials U [8,9] (first order mass operator) and are defined by

$$\bar{E}(q, K, k_F) = (q^2 + K^2) + \left(\frac{m}{\hbar^2} \right) \left\{ U(|\vec{q} + \vec{K}|) + U(|\vec{q} - \vec{K}|) \right\} . \quad (4)$$

The nuclear structure information is specified in terms of the one body density matrix elements (OBDME) (with α specifying the set n, l, j and $\tilde{a}_{\alpha m} = (-1)^{j-m} a_{\alpha -m}$)

$$S_{\alpha\alpha'I} = \left\langle J_f \left\| [a_{\alpha'}^\dagger \times \tilde{a}_\alpha]^I \right\| J_i \right\rangle \rightarrow \left\langle J \left\| [a_{\alpha'}^\dagger \times \tilde{a}_\alpha]^I \right\| J \right\rangle , \quad (5)$$

for the case of elastic scattering from a target of spin J . With the diagonal OBDME specified in the occupation number representation, for $I = 0$,

$$S_{\alpha\alpha 0} = \sqrt{2j + 1} \sigma_{\alpha\alpha} \quad (6)$$

where $\sigma_{\alpha\alpha}$ is the fractional shell occupancy with a filled shell signifying $\sigma_{\alpha\alpha} = 1$, the optical potential given by the folding process, takes the form

$$U(\vec{r}_1, \vec{r}_2; E) = \sum_{\alpha m \alpha' m'} (2j + 1) \sigma_{\alpha\alpha'} \times \left[\delta(\vec{r}_1 - \vec{r}_2) \int \varphi_{\alpha' m'}^*(\vec{s}) U^D(R_{1s}, E) \varphi_{\alpha m}(\vec{s}) d\vec{s} + \varphi_{\alpha' m'}^*(\vec{r}_1) U^{Ex}(R_{12}, E) \varphi_{\alpha m}(\vec{r}_2) \right], \quad (7)$$

where $R_{12} = |\vec{r}_1 - \vec{r}_2|$ and $R_{1s} = |\vec{r}_1 - \vec{s}|$, $\varphi_{\alpha m}$ are the single particle (SP) wave functions specifying the nucleons, and U^D and U^{Ex} are appropriate combinations of the multipoles of the effective interactions for the direct and exchange contributions to the optical potential respectively. The exchange term arises from the antisymmetry of the projectile and the struck (bound) nucleon within the nucleus.

The exchange terms are the major component of nonlocality in the NA optical potential. Indeed, neglect of those terms specifically in folding models leads to severe problems in the description of the observables [10], with the differential cross sections being overpredicted in some cases by up to several orders of magnitude. Another source of nonlocality is the NN interaction itself. In the calculation of g matrices, that nonlocality also contributes to that of the optical potential and manifests itself partly in the energy and density dependences in those g matrices. That it contributes to the overall nonlocal nature of the optical potential is also evident from the off-shell part of the g matrices. The extrapolations of the g matrices off-shell, relative to their on-shell values, are similar to those for the free NN t matrices [1], and so all aspects of the NN interaction are carried through in the solution of the BBG equations. We define such a model as g -folding.

It is clear from Eq. (2) that the appropriate form of the optical potential for pA and nA scattering calculations may be obtained from the common g matrix, with the projectile isospin allowing the selection of the correct components through the appropriate two-body isospin channels. The only addition in the case of pA scattering is the inclusion of the Coulomb interaction in Eq. (1).

The microscopic neutron and proton scattering predictions are compared with predictions from a phenomenological optical potential developed by Madland [11]. This potential is global in projectile energy, isospin, and target (Z, A), uses Woods-Saxon form factors, and was developed for use in a relativistic Schrödinger (relativistic kinematics) approach. The potential extends the earlier Schwandt work [12] by increasing the target mass range from $A = 24 - 208$ to $A = 12 - 208$, increasing the energy range from $E = 80 - 180$ MeV to $E = 50 - 400$ MeV, and transforming the Schwandt proton potential to a projectile-isospin dependent potential for neutrons and protons, using a relativistic Lane model naturally incorporating Coulomb effects. Experimental data for integrated observables (proton reaction, and neutron total cross sections) and proton elastic scattering angular distributions, were used to determine the phenomenological potential parameters. The potential is described in detail in Ref. [11].

The observables are obtained once the optical potential has been calculated, as is detailed in the recent review [1]. In particular, the integral observables are obtained from the S matrix, or equivalently the phase shifts, $\delta_l(k)$:

$$S_l^\pm \equiv S_l^\pm(k) = e^{2i\delta_l^\pm(k)} = \eta_l^\pm(k) e^{2i\Re[\delta_l^\pm(k)]} \quad (8)$$

where

$$\eta_l^\pm \equiv \eta_l^\pm(k) = |S_l^\pm(k)| = e^{-2\Im[\delta_l^\pm(k)]} . \quad (9)$$

In terms of these and with $E \propto k^2$, the elastic and total reaction (absorption) cross sections are given by

$$\begin{aligned} \sigma_{\text{el}}(E) &= \frac{\pi}{k^2} \sum_{l=0}^{\infty} \left\{ (l+1) |S_l^+ - 1|^2 + l |S_l^- - 1|^2 \right\} , \\ \sigma_R(E) &= \frac{\pi}{k^2} \sum_{l=0}^{\infty} \left\{ (l+1) \left[1 - (\eta_l^+)^2 \right] + l \left[1 - (\eta_l^-)^2 \right] \right\} , \end{aligned} \quad (10)$$

respectively. The total cross section, $\sigma_{\text{TOT}}(E)$, is the sum of these two cross sections.

III. RESULTS

Select results are presented for elastic 65 MeV NA scattering from ^{12}C , ^{28}Si , ^{40}Ca , ^{56}Fe , ^{90}Zr , and ^{208}Pb . We present the differential cross sections and analysing powers for all cases, as well as consider the integral neutron scattering data: the total, elastic, and total reaction cross sections. The shell model calculations, where applicable, were performed using the code OXBASH [13]. The starting NN interaction for the microscopic calculations was the Bonn B interaction [6].

The SP wave functions for the microscopic calculations were chosen to be harmonic oscillators, with the oscillator parameter chosen to reproduce the root-mean-square (r.m.s.) radius of each nucleus within the given shell model space. The exception to that was ^{208}Pb , for which we used a Skyrme-Hartree-Fock (SHF) calculation [14]. In that calculation, the neutron wave functions were chosen such that the difference in the neutron and proton r.m.s. radii were 0.16 ± 0.02 fm, the Friedman-Pandharipande neutron equation of state serving as the constraint. The choice of SHF wave functions reproduce both the proton and predicted neutron r.m.s. radius. For the other nuclei, Table I lists the oscillator parameter used for each nucleus along with the shell model used, and predicted r.m.s. radius. In all cases, the models used together with the choice of oscillator parameters reproduce the r.m.s. radii quite well. For all nuclei, these models and SP wave functions were used in the microscopic calculations of the scattering presented below.

The results of the microscopic calculations of the scattering from ^{12}C , as well as those obtained from the phenomenological model, are compared to the available data in Fig. 1. Therein, the proton scattering data of Kato *et al.* [15] and the neutron scattering data of Hjort *et al.* [16] (squares) and Ibaraki *et al.* [17] (diamonds) are compared to the results of the calculations made using the microscopic and phenomenological optical potentials. While the microscopic potential results tend to underestimate the region of the minimum ($\sim 40^\circ$), for both proton and neutron scattering from ^{12}C , the model reproduces well the overall shape and magnitude. The model also reproduces the analyzing powers well, and predicts the negative slope above 60° , which is not present in the result from the phenomenological calculation. For neutron scattering, the microscopic model gives much better agreement with the data for the forward angle cross section, and so one expects that the total cross

section would be better reproduced by this model. That total elastic cross section, along with the total reaction and total neutron scattering cross sections for all the nuclei, are given in Table II. As expected, the total cross section for n - ^{12}C scattering at 65 MeV is much better reproduced by the microscopic result. Also, there are differences between the predicted total elastic and total reaction cross sections. The microscopic model predicts a smaller elastic cross section and larger reaction cross section than the phenomenological model, suggesting the microscopic model calculates a weaker real and stronger imaginary part of the potential. Note that the total neutron scattering cross section from ^{12}C predicted by the microscopic model at intermediate energies is in good agreement with the data [3].

We compare the results of our calculations for the 65 MeV scattering of nucleons from ^{28}Si to the data in Fig. 2. The proton scattering data are those of Sakaguchi *et al.* [18], while the neutron data are those of Hjort *et al.* [16] and Ibaraki *et al.* [17]. The proton scattering data are described well by both models, the phenomenological model giving a better representation of both the cross section and analyzing power. There is a discrepancy between the two sets of neutron scattering data around the first minimum, at 25° . Both model results favor the Ibaraki set, giving excellent reproduction of those data, including in the region of the discrepancy. The models give similar results for the neutron analyzing power. In Table II, we find similar behavior in the optical potentials for ^{28}Si as for ^{12}C , as evidenced by the relative elastic and total reaction cross sections. Both models predict the total cross section to within 3%.

The differential cross sections and analyzing powers for the 65 MeV scattering of nucleons from ^{40}Ca are presented in Fig. 3. As with the previous results, both the microscopic and phenomenological results agree with the data of Sakaguchi *et al.* [18] quite well, with the phenomenology giving a better representation of the observables. However, as with ^{28}Si , both calculations are unable to reproduce the neutron scattering differential cross section data of Hjort *et al.* [16], in the region of the minimum, $\sim 23^\circ$. There are no other available data for this case with which to compare.

In Fig. 4, we compare the results of both model calculations for the scattering of 65 MeV nucleons from ^{56}Fe to the proton scattering data of Sakaguchi *et al.* [18], and to the neutron scattering data of Hjort *et al.* [16] and Ibaraki *et al.* [17]. The agreement between the model calculations and the data for proton scattering is quite good, and as before the phenomenological result gives the better representation of the data. As with ^{28}Si , a discrepancy between the Hjort and Ibaraki data sets exists in the region of the first minimum ($\sim 22^\circ$) of the neutron scattering differential cross section. The model calculations both favor the Ibaraki set. There would appear to be a normalization problem in the Hjort data in this region in general, when one considers also the previous examples. This would suggest the need for another measurement of these data in order to resolve the discrepancy. In the case of the neutron integral observables, the optical potentials for ^{56}Fe reflect the same behavior as for the lighter systems, although in this case the predicted total cross sections are in agreement.

The results of both model calculations for the 65 MeV scattering of nucleons from ^{90}Zr are compared to the proton scattering data of Sakaguchi *et al.* [18] and neutron scattering data of Ibaraki *et al.* [17] in Fig. 5. There is good agreement between the model results and the data. This is also reflected in the total cross section, for which both models are in agreement with the measured value to within 1%. However, we would encourage measurement of the

neutron analyzing power in this case. That analyzing power as predicted by both models is very much different to the proton one, unlike those of the lighter nuclei. This is an effect that was first observed by Kozack and Madland [4] for 100 MeV nucleon scattering from ^{208}Pb , and confirmed recently by Karataglidis and Madland [5] using the microscopic Schrödinger model.

In Fig. 6, the results of the model calculations for the 65 MeV scattering of nucleons from ^{208}Pb are compared to the proton scattering data of Sakaguchi *et al.* (circles) [18] and the neutron scattering data of Hjort *et al.* [16] (squares) Ibaraki *et al.* [17] (diamonds). While both models give a reasonable representation of the proton scattering data, with the phenomenological model doing better, the neutron scattering data are far better reproduced by the microscopic model. The phenomenological model significantly underpredicts the cross section above 20° . In Fig. 7, we show the total and total reaction cross sections for the scattering of neutrons from ^{208}Pb . Between 60 and 200 MeV the predicted total cross section as calculated by the microscopic model shows excellent agreement, to within 1.5%, with the data of Finlay *et al.* [3,19]. The phenomenological model does reasonably well above 80 MeV, underpredicting the total cross section by at most 4%. Below 80 MeV, however, the phenomenological model fails to reproduce the minimum. This is consistent with the relatively poor results of the phenomenological model at 65 MeV. As the elastic cross section is well reproduced by the microscopic model, one has confidence in the predicted microscopic results of the total reaction cross section. Those measurements rely on careful subtraction of the elastic from the total cross section and hence some degree of error is to be expected. That we can predict the reaction cross section to within 10% of measurement is encouraging. The phenomenological model does worse. Note that unlike the optical potentials for the other nuclei, we find a weaker imaginary part of the microscopic optical potential relative to that of the phenomenological.

As with the results of Kozack and Madland [4], which were based on a relativistic Dirac phenomenological optical potential model, and of Karataglidis and Madland, as based on the microscopic Schrödinger model [5], we observe a significant difference between the proton and neutron analyzing powers for the 65 MeV scattering from ^{208}Pb . The analyzing powers are not completely out of phase, however, as was observed in the other calculations at 100 MeV, suggesting an energy dependence.

IV. CONCLUSIONS

We have presented detailed comparisons of model predictions of proton and neutron elastic scattering at 65 MeV for a number of nuclei. The models used were a phenomenological relativistic model and a microscopic one based on the g matrices of the Bonn-B NN interaction.

In all cases, the differential cross sections and analyzing powers were well reproduced by both models. This is of note as the microscopic optical potentials for both proton and neutron scattering are derived from the same g matrix, with isospin selecting the appropriate components. Thus the changes in magnitude and shape between the proton and neutron scattering observables are contained within the same underlying physics. While the phenomenological potentials are derived within a relativistic Lane model, those potentials

rely on a global fit to constrain parameters and hence differences between the proton and neutron potentials. Those differences are naturally contained in the microscopic model.

Both the microscopic and phenomenological model analyses contained herein have allowed us to identify a problem with the existing set of neutron scattering data. The two sets of data (Hjort *et al.* [16] and Ibaraki *et al.* [17]) show a discrepancy between them in the region of the first minimum. The analyses favor the Ibaraki data and, as the two approaches to the scattering problem are fundamentally different, one has some confidence in the results. A new measurement would be required of these data, especially of the n - ^{40}Ca elastic scattering cross section.

Measurements of the neutron scattering analyzing powers are also suggested. First, the differences between the two models are most noticeable in the results for the neutron analyzing powers, suggesting a method of delineation between the two. Second, for the heavier nuclei, a significant difference is observed between the proton and neutron analyzing powers. That difference is attributed to the absence of the Coulomb potential in neutron scattering [4]. A measurement of the neutron analyzing power for scattering from ^{90}Zr or ^{208}Pb at intermediate energies, admittedly a difficult experiment, would demonstrate this effect, and a systematic study based on the microscopic model is under way to determine in which cases this effect would be strongest [20].

This work was supported by the United States Department of Energy Contract no. W-7405-ENG-36.

REFERENCES

- [1] K. Amos, P. J. Dortmans, H. V. von Geramb, S. Karataglidis, and J. Raynal, *Adv. in Nucl. Phys.* **25** (2000), 276.
- [2] P. J. Dortmans, K. Amos, S. Karataglidis, and J. Raynal, *Phys. Rev. C* **58**, 3002 (1998).
- [3] P. K. Deb, K. Amos, S. Karataglidis, M. B. Chadwick, and D. G. Madland, *Phys. Rev. Lett.* **86**, 3248 (2001).
- [4] R. Kozack and D. G. Madland, *Nucl. Phys.* **A509**, 664 (1990).
- [5] S. Karataglidis and D. G. Madland (2001), submitted for publication to *Phys. Rev. Lett.*, nucl-th/0103048.
- [6] R. Machleidt, K. Holinde, and C. Elster, *Phys. Rep.* **149**, 1 (1987).
- [7] J. Raynal, *computer code DWBA98* (1999), (NEA 1209/05).
- [8] M. Haftel and F. Tabakin, *Nucl. Phys.* **A158**, 1 (1970).
- [9] P. J. Dortmans and K. Amos, *J. Phys. G* **17**, 901 (1991).
- [10] P. K. Deb and K. Amos, *Phys. Rev. C* **62**, 024605 (2000).
- [11] D. G. Madland, in *Nucleon-nucleus optical model up to 200 MeV* (NEA/OECD, 1997), p. 129.
- [12] P. Schwandt, H. O. Meyer, W. W. Jacobs, A. D. Bacher, S. E. Vigdor, M. D. Kaitchuck, and T. R. Donoghue, *Phys. Rev. C* **26**, 55 (1982).
- [13] OXBASH-MSU (the Oxford-Buenos-Aries-Michigan State University shell model code). A. Ecthegoyen, W. D. M. Raye, and N. S. Godwin (MSU version by B. A. Brown, 1986); B. A. Brown, A. Etchegoyen, and W. D. M. Rae, MSUCL Report Number 524, 1986 (unpublished).
- [14] B. A. Brown, *Phys. Rev. Lett.* **85**, 5296 (2000).
- [15] S. Kato *et al.*, *Phys. Rev. C* **31**, 1616 (1985).
- [16] E. L. Hjort, F. P. Brady, J. L. Romero, J. R. Drummond, D. S. Sorenson, J. H. Osborne, B. McEachern, and L. F. Hansen, *Phys. Rev. C* **50**, 275 (1994).
- [17] M. Ibaraki, M. Baba, T. Miura, Y. Hirasawa, Y. Nauchi, H. Nakashima, S. Meigo, O. Iwamoto, and S. Tanaka, *Nucl. Inst. Meth. Phys. Res.* **A446**, 536 (2000), M. Baba, private communication.
- [18] H. Sakaguchi, M. Nakamura, K. Hatanaka, A. Goto, T. Noro, F. Ohtani, H. Sakamoto, H. Ogawa, and S. Kobayashi, *Phys. Rev. C* **26**, 944 (1982).
- [19] R. W. Finlay, W. P. Abfalterer, G. Fink, E. Montei, T. Adami, P. W. Lisowski, G. L. Morgan, and R. C. Haight, *Phys. Rev. C* **47**, 237 (1993).
- [20] S. Karataglidis and D. G. Madland (to be published).
- [21] H. de Vries, C. W. de Jager, and C. de Vries, *At. Data Nucl. Data Tables* **36**, 495 (1987).
- [22] E. K. Warburton and B. A. Brown, *Phys. Rev. C* **46**, 923 (1992).
- [23] B. A. Brown and B. H. Wildenthal, *Ann. Rev. Nucl. Part. Sci.* **36**, 29 (1988).
- [24] W. A. Richter, M. G. van der Merwe, R. E. Julies, and B. A. Brown, *Nucl. Phys.* **A523**, 325 (1991).
- [25] X. Ji and B. H. Wildenthal, *Phys. Rev. C* **40**, 389 (1989).
- [26] M. H. MacGregor, W. P. Ball, and R. Booth, *Phys. Rev.* **111**, 1155 (1958).
- [27] R. G. P. Voss and R. Wilson, *Proc. Roy. Soc. A* **236**, 52 (1956).
- [28] J. Dejuren and N. Knable, *Phys. Rev.* **77**, 606 (1950).
- [29] T. W. Bonner and J. H. Slattery, *Phys. Rev.* **113**, 1088 (1959).
- [30] J. G. Degtjarev and V. G. Nadtochij, *Sov. J. Nucl. Phys.* **11**, 1043 (1962).

TABLES

TABLE I. Shell model space, interaction, harmonic oscillator parameter (b) and r.m.s. radii for the nuclei listed.

Nucleus	Model space	Interaction	b (fm)	r_{rms} (fm)	
				(Theory)	(Expt [21])
^{12}C	$(0 + 2)\hbar\omega$	WBT [22]	1.67	2.448	2.472 ± 0.015
^{28}Si	$0\hbar\omega$	USD [23]	1.85	3.088	3.086 ± 0.018
^{40}Ca	$0\hbar\omega$	packed	2.00	3.464	3.482 ± 0.025
^{56}Fe	$0\hbar\omega^a$	FPD6 [24]	2.05	3.796	3.801 ± 0.015
^{90}Zr	NISJ	NISJ [25]	2.15	4.27	4.258 ± 0.008

^a A 2p-2h fp -shell model built on the minimal fp -space wave function.

TABLE II. Elastic, total reaction, and total cross sections for the scattering of 65 MeV neutrons from the nuclei given. The microscopic and phenomenological results are denoted by MOMP and POMP, respectively.

Nucleus	σ_{el} (b)		σ_R (b)		σ_{TOT} (b)		Expt. [19]
	MOMP	POMP	MOMP	POMP	MOMP	POMP	
^{12}C	0.417	0.537	0.331	0.269	0.748	0.806	0.753 ± 0.005
^{28}Si	0.852	0.988	0.598	0.523	1.450	1.511	1.500 ± 0.006^a
^{40}Ca	1.122	1.235	0.788	0.690	1.910	1.925	1.966 ± 0.009
^{56}Fe	1.370	1.465	0.964	0.890	2.334	2.355	—
^{90}Zr	1.714	1.847	1.299	1.272	3.013	3.119	3.048 ± 0.003
^{208}Pb	2.415	2.661	2.195	2.339	4.610	5.000	4.635 ± 0.001

^a A natural target was used.

FIGURES

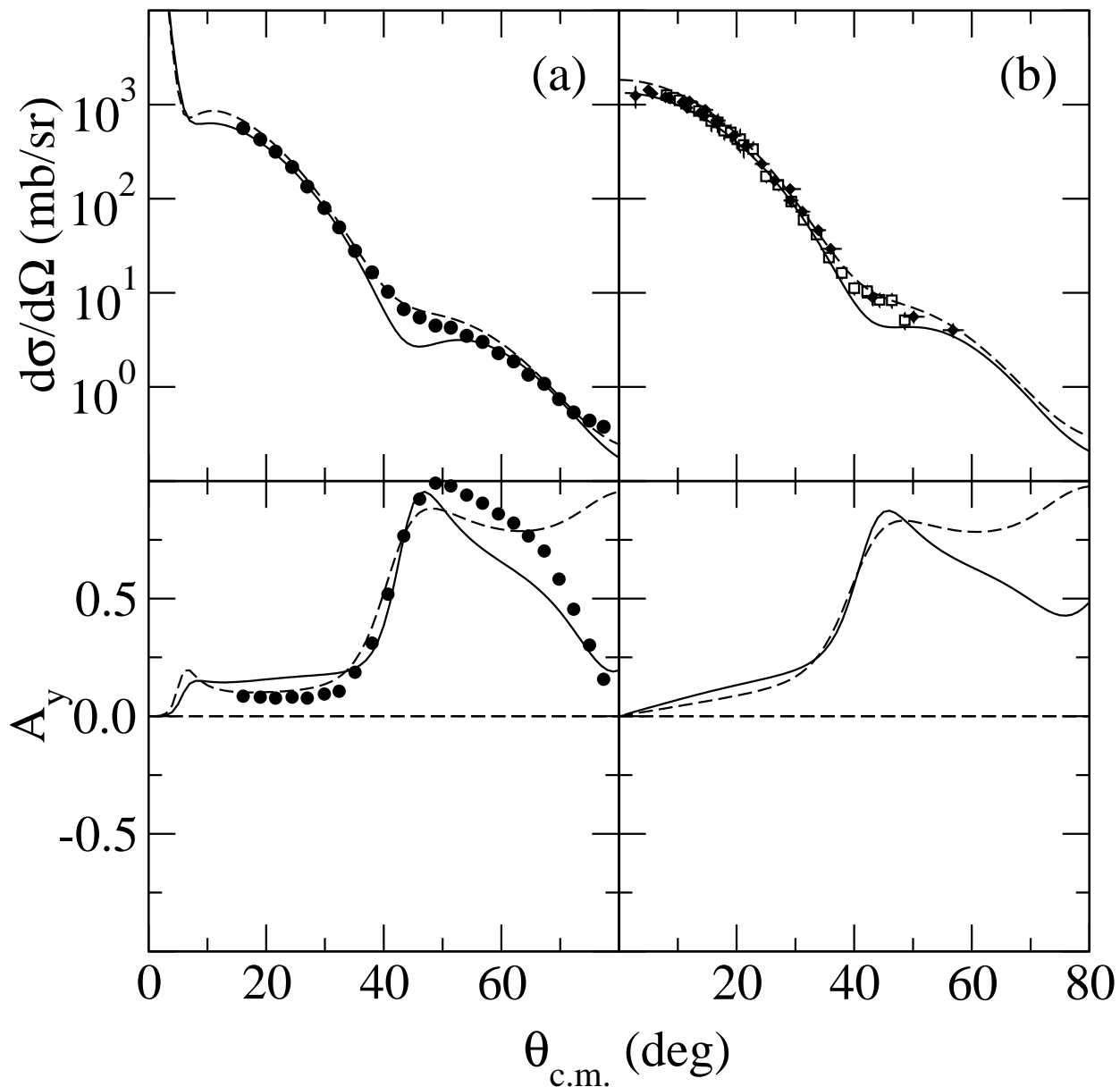


FIG. 1. Differential cross sections and analysing powers for the scattering of 65 MeV protons (a) and neutrons (b) from ^{12}C . The proton scattering data of Kato *et al.* [15] (circles), and the neutron scattering data of Hjort *et al.* (squares) [16] and Ibaraki *et al.* (diamonds) [17] are compared to the results of the calculations made using the microscopic (solid line) and phenomenological (dashed line) optical potentials.

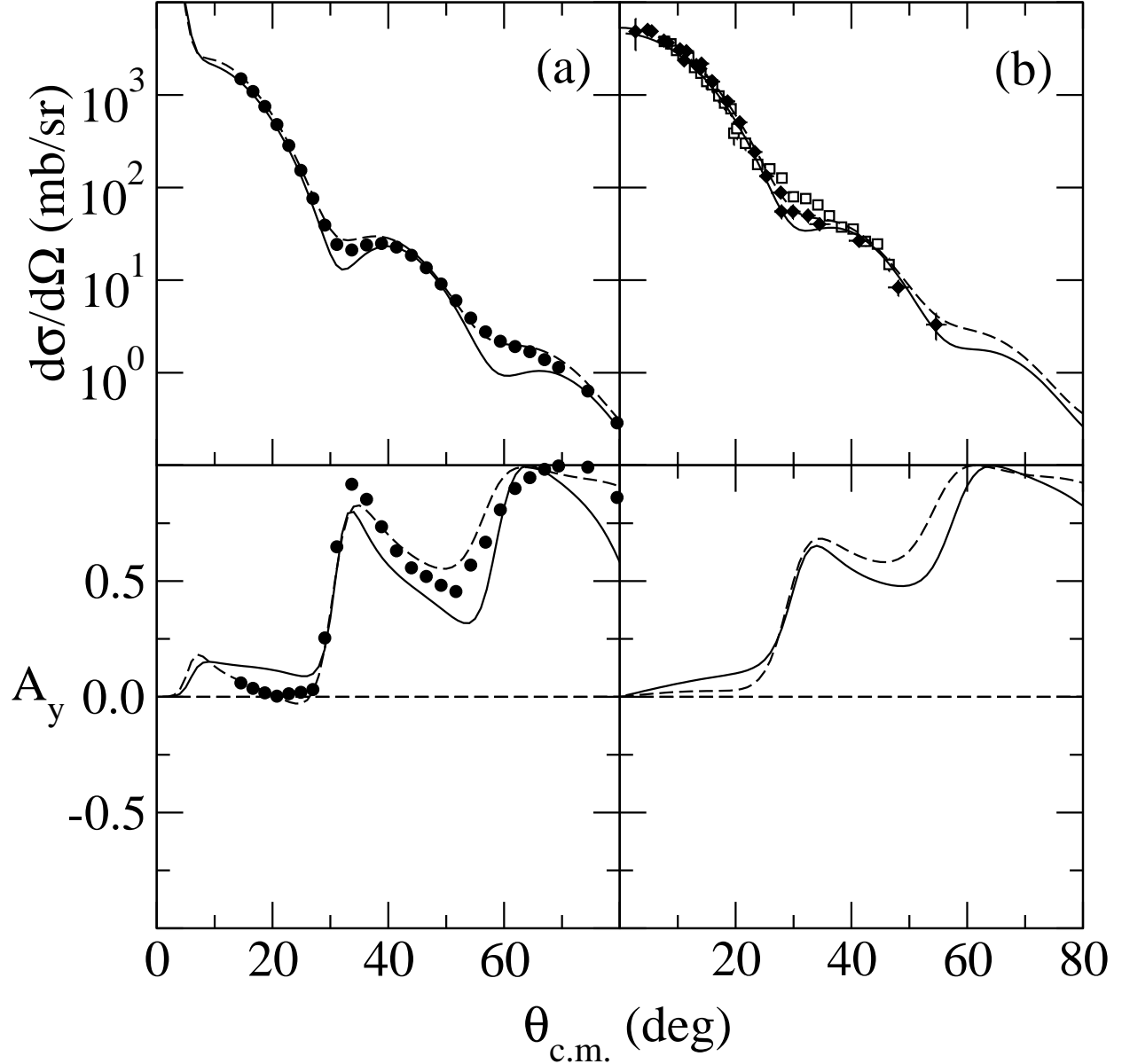


FIG. 2. As for Fig. 1, but for ^{28}Si . The proton scattering data [circles, (a)] are those of Sakaguchi *et al.* [18], while the neutron scattering data (b) are from Hjort *et al.* [16] (squares) and Ibaraki *et al.* [17] (diamonds).

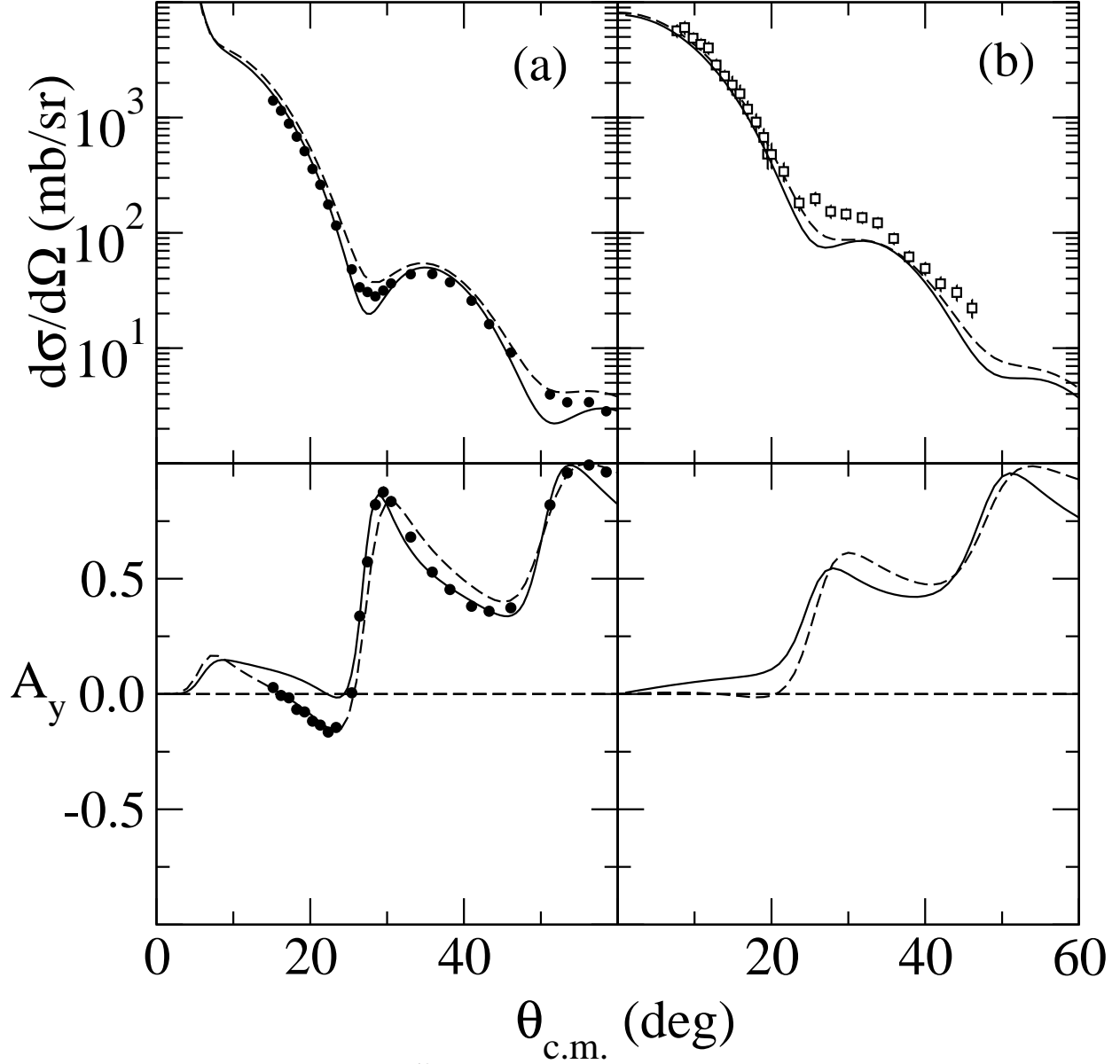


FIG. 3. As for Fig. 1, but for ^{40}Ca . The proton scattering data [circles, (a)] are those of Sakaguchi *et al.* [18]. The neutron data scattering (b) are those of Hjort *et al.* [16] (squares).

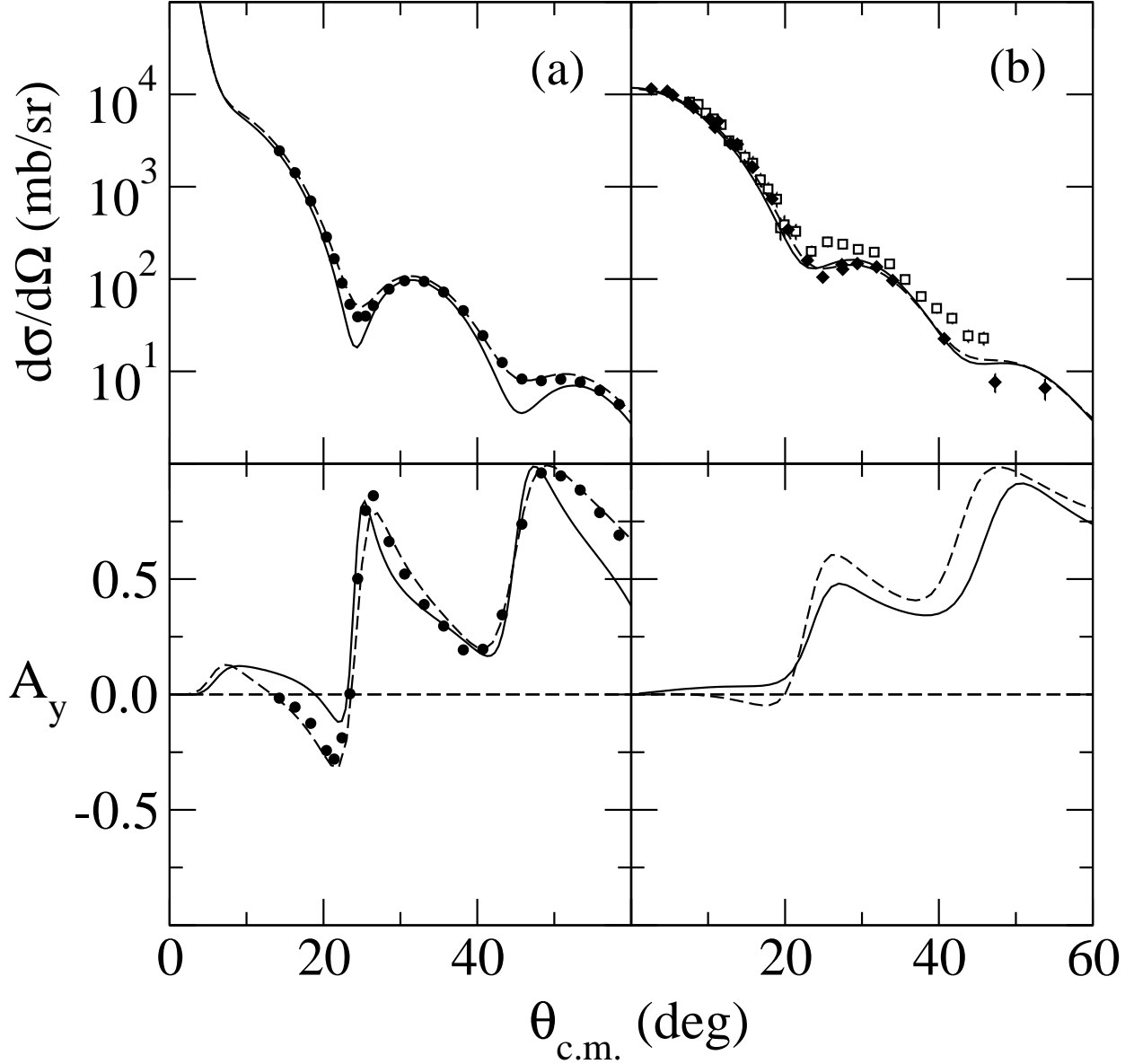


FIG. 4. As for Fig. 1, but for ^{56}Fe . The proton scattering data [circles, (a)] are those of Sakaguchi *et al.* [18], while the neutron scattering data in (b) are those of Hjort *et al.* [16] (squares) and Ibaraki *et al.* [17] (diamonds).

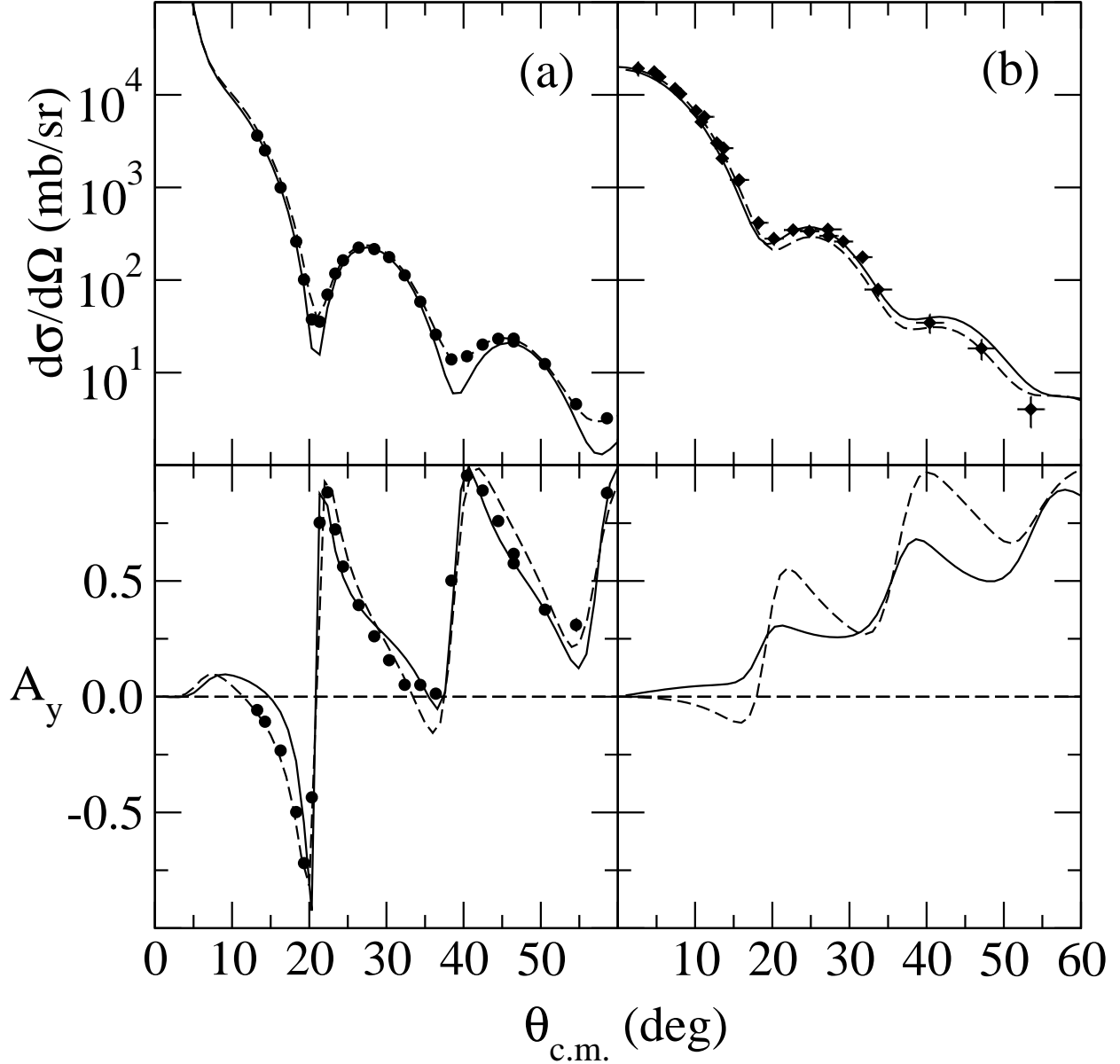


FIG. 5. As for Fig. 1, but for ^{90}Zr . The proton scattering data [circles, (a)] are those of Sakaguchi *et al.* [18], while the neutron scattering data in (b) are those of Ibaraki *et al.* [17] (diamonds).

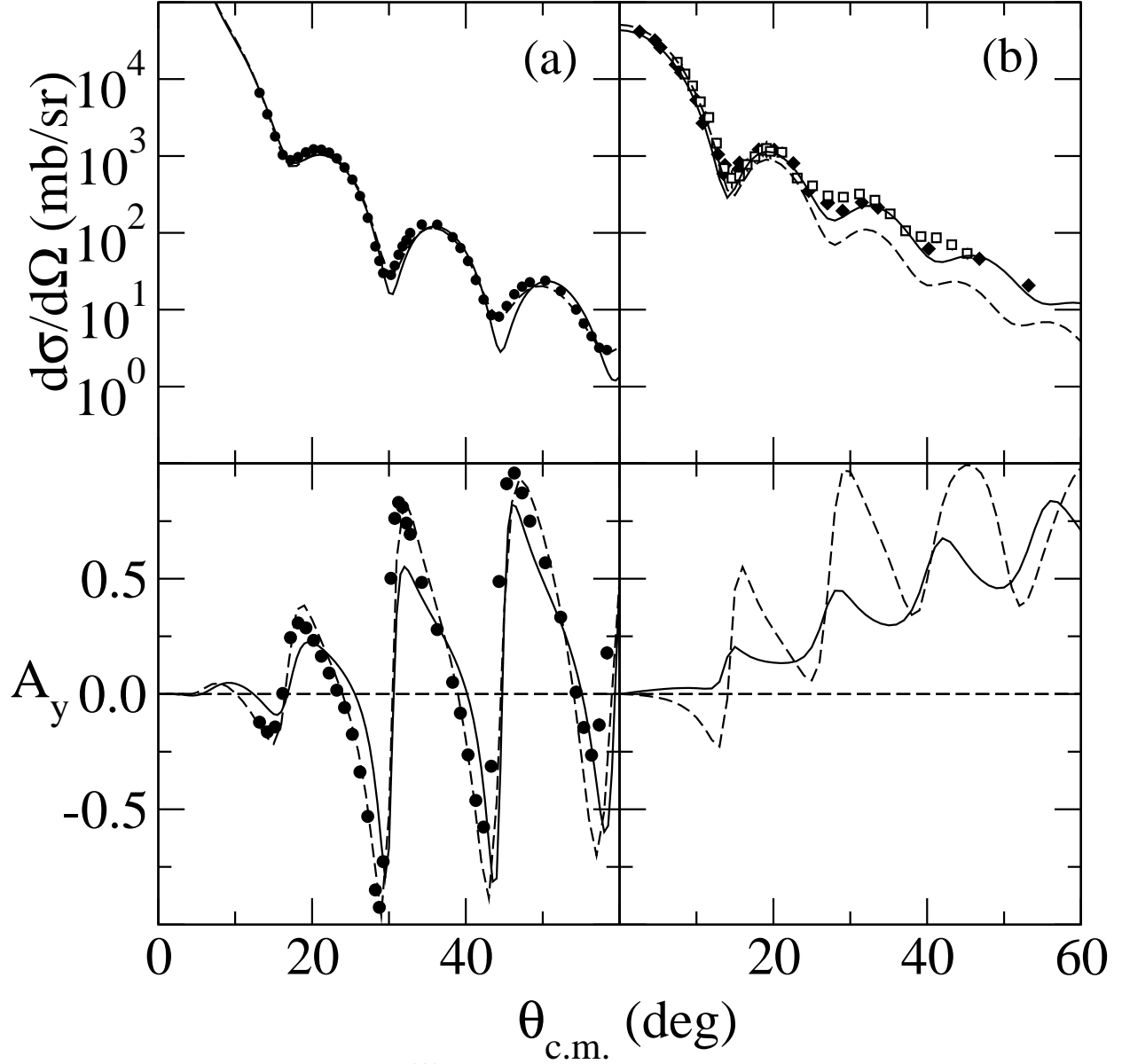


FIG. 6. As for Fig. 1, but for ^{208}Pb . The proton scattering data [circles, (a)] are those of Sakaguchi *et al.* [18], while the neutron scattering data in (b) are those of Hjort *et al.* [16] (squares) Ibaraki *et al.* [17] (diamonds).

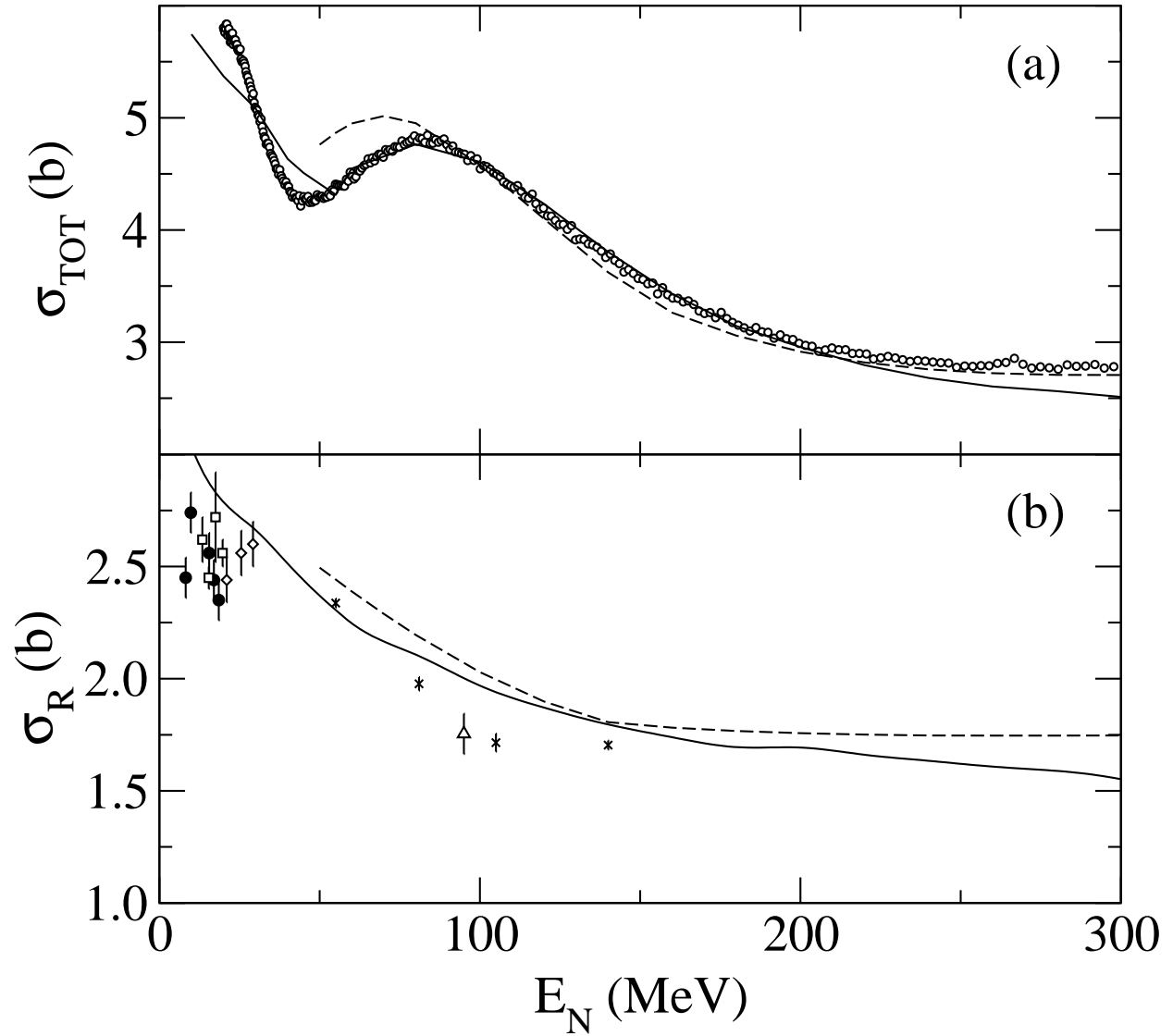


FIG. 7. Total and total reaction cross sections, displayed in (a) and (b) respectively, for the scattering of neutrons from ^{208}Pb . The total cross section data of Findlay *et al.* (open circles) and total reaction cross section data [26–30] are compared to the results of the microscopic (solid line) and phenomenological (dashed line) calculations.